Nanoscale Horizons

ROYAL SOCIETY OF CHEMISTRY

COMMUNICATION

View Article Online
View Journal | View Issue

Cite this: *Nanoscale Horiz.*, 2020, 5, 1332

Received 5th May 2020,
Accepted 23rd July 2020

DOI: 10.1039/d0nh00263a

rsc.li/nanoscale-horizons

Effect of alkaline earth metal chloride additives BCl_2 (B = Mg, Ca, Sr and Ba) on the photovoltaic performance of $FAPbI_3$ based perovskite solar cells†

Mei Lyu, Do-Kyoung Lee and Nam-Gyu Park *

Additive engineering is known to be an effective method for inducing a simultaneous effect of enlarging the grain size and surface passivation. As compared to the monovalent halides frequently used as additives, divalent halides are relatively less investigated in the role of additives. In this work, we report effects of alkaline earth metal halides BCl_2 (B = Mg, Ca, Sr, Ba) as additives on the opto-electronic properties and photovoltaic performance of $FAPbI_3$ based perovskite solar cells (PSCs). A significant improvement in power conversion efficiency (PCE) from 17.27% to 21.11% is observed by $MgCl_2$ addition in the $FAPbI_3$ precursor solution, while a marginal increment for $CaCl_2$ or $BaCl_2$ and a negative effect for $SrCl_2$ is observed. The lattice constant of cubic $FAPbI_3$ is hardly changed by additives, while the crystallinity is improved by $MgCl_2$. The carrier lifetime increases from 40 ns to 287 ns and the trap density is reduced from 1.08×10^{16} cm^{-3} to 3.19×10^{15} cm^{-3} by addition of 5 mol% $MgCl_2$, which is responsible for the enhancement in photovoltaic parameters. The steady-state PCE of the PSC with the $MgCl_2$-additive-treated $FAPbI_3$ measured under continuous illumination at the maximum power point remains unchanged for 1500 s.

New concepts

Formamidinium lead iodide ($FAPbI_3$) perovskite is known to be an ideal material among the studied compositions in terms of optical bandgap. The precursor solution is suggested to include an additive – normally, the monovalent cationic chlorides, such as MACl or CsCl, are frequently used as additives – to improve the photovoltaic performance of $FAPbI_3$ perovskite solar cells (PSCs). However, a change in bandgap is expected because MA or Cs cations can replace the FA cations. Thus, it is required to keep the bandgap of $FAPbI_3$ even after modification by additive engineering. As compared to the monovalent halides, no systematic investigation on the role of divalent halides has been reported in $FAPbI_3$ based PSCs. In this work, we first report the effects of alkaline earth metal halide BCl_2 (B = Mg, Ca, Sr, Ba) additives on the opto-electronic properties and photovoltaic performance of $FAPbI_3$ based PSCs. We have found that the addition of $MgCl_2$ improves the power conversion efficiency significantly due to a large increase in carrier lifetime and a significant reduction in trap density. In addition, no change in bandgap is observed because of the higher oxidation state and much smaller ionic radius of Mg^{2+} than FA and Pb cations.

Introduction

Since the report of a 9.7% efficient and 500 h stable solid-state perovskite solar cell (PSC) in 2012,[1] developed to solve the instability of methylammonium lead iodide ($MAPbI_3$) in a liquid electrolyte,[2,3] a swift surge in perovskite photovoltaics led to a certified power conversion efficiency (PCE) of 25.2% in 2019.[4] The inherently excellent opto-electronic properties of organic lead halide perovskites[5–7] are responsible for the superb photovoltaic performance, which might be better than the well-known thin film solar cell materials such as $Cu(In_{1-x}Ga_x)Se_2$, multi-crystalline Si and CdTe because of higher PCE. Among the studied compositions for PSCs, $FAPbI_3$ (FA = formamidnium) has been regarded as an ideal perovskite because of suitable bandgap (~1.47 eV) and no structural phase transition at the operating temperature.[8] However, the photoactive $FAPbI_3$ is known to be in the high-temperature stabilized α phase, and tends to undergo phase transition from α to photo-inactive δ phase at ambient temperature.[9] It was first reported that a substitution of a certain amount of FA cations with Cs cations can stabilize the α phase at ambient temperature.[10] In general, substitution with smaller monovalent cations (Cs^+, Rb^+ or MA) and/or halide anion (Br^-) was found to stabilize the α phase of $FAPbI_3$ thermodynamically.[11–14] Thus, these cations can be referred to as "stabilizers" in $FAPbI_3$.[12]

The stabilizers can be incorporated compositionally by stoichiometrically mixing FA with a certain amount of stabilizer, which is called "compositional engineering". The incorporation of stabilizer is also possible by "additive engineering" in which an adequate amount of additive is mixed with $FAPbI_3$ precursor. The difference between compositional engineering

School of Chemical Engineering, Sungkyunkwan University, Suwon 16419, Korea. E-mail: npark@skku.edu

† Electronic supplementary information (ESI) available. See DOI: 10.1039/d0nh00263a

and additive engineering is that additive engineering is a non stoichiometric approach and elements that may not be involved in the composition can be used as additives. Additive engineering has been found to be also beneficial for both surface passivation and growth of grain size.[15] It is well-known that addition of MACl additive in a perovskite precursor solution shows a positive effect on the photovoltaic performance of $FAPbI_3$ based PSCs.[16–18] Although it has been argued whether or not chloride is incorporated in iodide sites, it is widely accepted that chloride plays an important role in enlarging the grain size and improving crystallinity.[19] Since there is a positive effect of chloride in additives, we have been motivated to systematically investigate the effect of divalent alkaline earth metal chlorides, BCl_2 (B = Mg, Ca, Sr and Ba), on the photovoltaic performance and stability of $FAPbI_3$ based PSCs. Since the divalent cations in BCl_2 are smaller in ionic radius (Mg^{2+} = 72 pm, Ca^{2+} = 100 pm, Sr^{2+} = 118 pm, and Ba^{2+} = 135 pm) and have higher formal charge than the FA cation, the surface passivation effect is expected rather than the substitution effect. In addition, the chloride content of BCl_2 is twice that of monovalent chloride when the same quantity is dissolved in the precursor solution, which may also affect the opto-electronic properties of the PSCs. To the best of our knowledge, no systematic studies have been reported on the additive engineering of $FAPbI_3$ with BCl_2.

Here, we report on the effects of BCl_2 additives on the photovoltaic parameters and opto-electronic properties of the $FAPbI_3$ based PSCs. The additive BCl_2 is mixed with a pre-synthesized $FAPbI_3$ powder,[20] where the concentration of BCl_2, $[BCl_2]$, is varied with respect to $[FAPbI_3]$. Among the studied additives, $MgCl_2$ is found to improve the photovoltaic performance and stability. Crystal structure, film morphology, band alignment and carrier lifetime are comparatively investigated to understand the basis for the improvement. A pristine $FAPbI_3$ device shows a PCE of 17.27% which is significantly improved to 21.11% by addition of $MgCl_2$ in the $FAPbI_3$ precursor solution.

Results and discussion

Effect of BCl_2 (B = Mg, Ca, Sr and Ba) on the opto-electronic properties of $FAPbI_3$ and photovoltaic performance

The perovskite precursor solutions are prepared by mixing the pre-synthesized $FAPbI_3$ powder (yellow δ phase) with BCl_2 with different molar ratios (see Experimental details). In order to investigate how the metal precursor additives change the reactivity of the perovskite precursors, UV-vis absorption spectroscopy of the precursor solution is studied. Fig. S1 (ESI†) shows that the absorption band around 310 nm is due to the iodoplumbate (probably $PbI_2(DMF)_x(DMSO)_{4-x}$ species), where peak intensity is higher for the $MgCl_2$ additive than for other additives. A strong absorption is indicative of an increase in iodoplumbate concentration and thereby an improvement of photovoltaic performance.[21] Another weak absorption peak at around 380 nm (inset in Fig. S1, ESI†) is related to PbI_3^-.[22] This peak is also relatively intense for the $MgCl_2$ additive compared to other additives. When considering that two characteristic peaks in the precursor solution affect the photovoltaic performance, $MgCl_2$ additive is expected to be better in performance than other additives, which will be further evaluated. Fig. 1 shows a schematic illustration of perovskite deposition, where the precursor solution with and without additive is spin-coated on a SnO_2 coated FTO (fluorine-doped tin oxide) substrate. To control the crystal growth, an intermediate is formed by dripping diethyl ether during the spin-coating procedure.[23] The thickness of the 150 °C-annealed perovskite film is about 440 nm as confirmed from cross-sectional scanning electron microscopy (SEM) (images not shown).

The effects of the concentration of the additives on the photovoltaic parameters are investigated. As shown in Fig. S2 (ESI†), the photovoltaic parameters are strongly dependent on the additive concentration (note that the final concentration may be different because the solution was filtered prior to use), from which an optimal concentration is determined to be 5 mol% for $MgCl_2$, 1 mol% for $CaCl_2$ and 9 mol% for $BaCl_2$. In contrast to the Mg, Ca and Ba cases, the addition of $SrCl_2$ additive lowers the photovoltaic performance. Despite the negative effect of $SrCl_2$, 10 mol% shows better performance among the tested concentrations from 5 mol% to 15 mol%. Fig. 2 shows the statistical short-circuit photocurrent density (J_{sc}), open-circuit voltage (V_{oc}), fill factor (FF) and power conversion efficiency (PCE) for the optimal concentration of BCl_2 additives. Unlike the BI_2 additives doped in $MAPbI_3$,[24,25] 5 mol% $MgCl_2$ improves substantially V_{oc} and FF, while a negligible or slight enhancement is observed for $CaCl_2$ and $BaCl_2$. Mean values are listed in Table 1, where the average PCE estimated from the

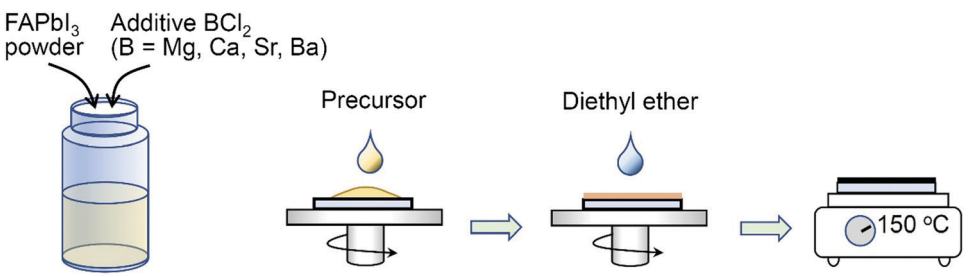

Fig. 1 A schematic illustration of the perovskite deposition procedure. The precursor solution was prepared by mixing the pre-synthesized $FAPbI_3$ powder with BCl_2 additive (B = Mg, Ca, Sr and Ba), which was spin-coated. Diethyl ether was dipped for 20 s after rotating the substrate. The film was annealed at 150 °C in an air atmosphere.

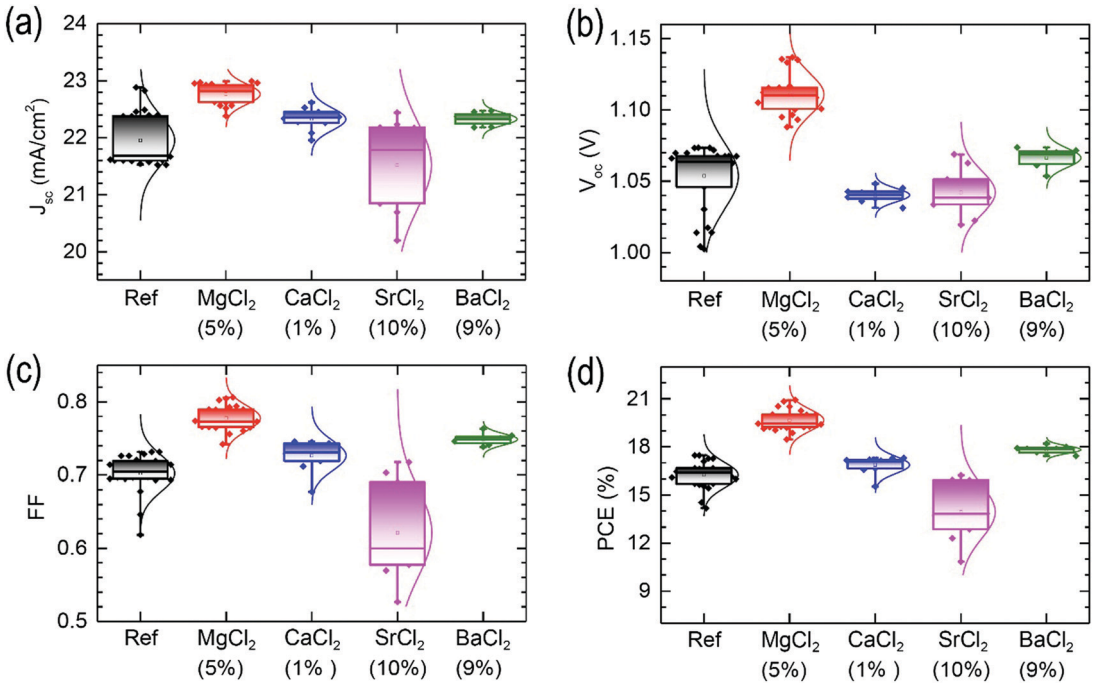

Fig. 2 Statistical photovoltaic parameters of (a) J_{sc}, (b) V_{oc}, (c) FF and (d) PCE measured at reverse scan for the BCl_2 additives (B = Mg, Ca, Sr and Ba). Values in parentheses are the optimal mol% of the additive with respect to $FAPbI_3$.

Table 1 Mean photovoltaic parameters of PSCs employing $FAPbI_3$ perovskite films with and without (Ref) BCl_2 additives (B = Mg, Ca, Sr and Ba). FS and RS stand for forward scan and reverse scan, respectively

Additive (mol%)		J_{sc} (mA cm^{-2})	V_{oc} (V)	FF	PCE (%)
Ref (w/o)	FS	21.84 ± 0.42	1.07 ± 0.01	0.72 ± 0.03	16.66 ± 1.06
	RS	21.97 ± 0.68	1.05 ± 0.03	0.71 ± 0.03	16.38 ± 1.02
$MgCl_2$ (5%)	FS	22.72 ± 0.41	1.11 ± 0.02	0.77 ± 0.02	19.36 ± 0.98
	RS	22.76 ± 0.31	1.11 ± 0.02	0.78 ± 0.03	19.67 ± 1.23
$CaCl_2$ (1%)	FS	22.37 ± 0.33	1.05 ± 0.01	0.72 ± 0.04	16.86 ± 0.89
	RS	22.11 ± 0.33	1.04 ± 0.01	0.70 ± 0.03	16.09 ± 0.88
$SrCl_2$ (10%)	FS	21.57 ± 1.12	1.04 ± 0.03	0.57 ± 0.13	12.75 ± 3.70
	RS	21.52 ± 1.12	1.04 ± 0.02	0.62 ± 0.10	13.95 ± 2.69
$BaCl_2$ (9%)	FS	22.21 ± 0.43	1.07 ± 0.01	0.75 ± 0.01	17.66 ± 0.40
	RS	22.33 ± 0.15	1.07 ± 0.01	0.75 ± 0.01	17.82 ± 0.39

reverse scanned parameters is improved from 16.39% to 19.66% by $MgCl_2$ addition. A large improvement in V_{oc} and FF implies that recombination might be reduced by the $MgCl_2$ additive. In our study, bulk doping in $FAPbI_3$ with $SrCl_2$ shows a negative effect leading to deterioration of the photovoltaic performance, which is in contrast to the previous work reporting an improved PCE by the 10–30% doping with $SrCl_2$ in $MAPbI_3$ and even the 2% doping with SrI_2 in $CsPbI_3$.[26,27]

Surface morphology is not significantly altered by $MgCl_2$, while $CaCl_2$, $SrCl_2$ and $BaCl_2$ change the surface morphology of $FAPbI_3$ (Fig. 3(a–e)). Cross-sectional SEM images confirm that $MgCl_2$ results in a pinhole-free interface between SnO_2 and perovskite, whereas large pinholes are formed at the interface for the pristine $FAPbI_3$. This indicates that the $MgCl_2$ additive supports an underlying conformal growth of perovskite on the substrate. The $MgCl_2$ additive is expected to contribute to the enlargement of the grain size of $FAPbI_3$ perovskite due to the higher coordination interaction between FA^+ and Mg^{2+} than those of FA^+ and Pb^{2+} [28,29] and/or retarded crystallization kinetics.[30] The higher J_{sc} obtained from the $MgCl_2$ additive is thus probably due to better charge collection owing to the pinhole-free interface. In addition, the crystallinity of α phase $FAPbI_3$ is improved in the presence of $MgCl_2$ as confirmed from the X-ray diffraction (XRD) pattern in Fig. 3(f), which might be associated with higher V_{oc} and FF because of the long-range ordering of $FAPbI_3$ and thereby less defects. On the other hand, the addition of $CaCl_2$, $SrCl_2$ and $BaCl_2$ cannot fully convert the δ phase to α phase because the δ phase is still present in the annealed film (Fig. 3(g)). Moreover, the $CaCl_2$ additive increases the unreacted PbI_2 peak, implying a strong interaction between $CaCl_2$ and PbI_2 in the precursor solution. Although the ionic radius of Sr^{2+} (118 pm) is similar to that of Pb^{2+} (119 pm), Sr^{2+} is not likely to replace Pb^{2+} because unreacted $SrCl_2$ exists in the annealed film as shown in the XRD peak at around 12.8° in Fig. 3(g) and the lattice constant of cubic $FAPbI_3$ [31] is unchanged by $SrCl_2$ due to no peak shift in the (100) reflection at $2\theta = 13.94°$.

Energy dispersive X-ray spectroscopy (EDS) is carried out to investigate the presence of BCl_2 in the annealed $FAPbI_3$ film. For the $MgCl_2$ case in Fig. 4(a), neither Mg nor Cl is detected on the film surface. Similarly, Ca and Cl are not detected on the film surface for $FAPbI_3$ with $CaCl_2$ additive (Fig. 4(b)). However, for the $SrCl_2$ and $BaCl_2$ cases, Sr, Ba and Cl elements are detected with an atomic ratio of Sr : Cl or Ba : Cl = 1 : 2 (Fig. 4(c) and (d)). No detection of $MgCl_2$ and $CaCl_2$ is probably due to the relatively lower concentration as compared to $SrCl_2$ and $BaCl_2$. The ratio of I to Pb is found to be almost 3 (atomic ratio I : Pb = 18.86 : 6.16) for the $MgCl_2$ case, which is indicative of stoichiometric formation of $FAPbI_3$. On the other hand, iodide-rich

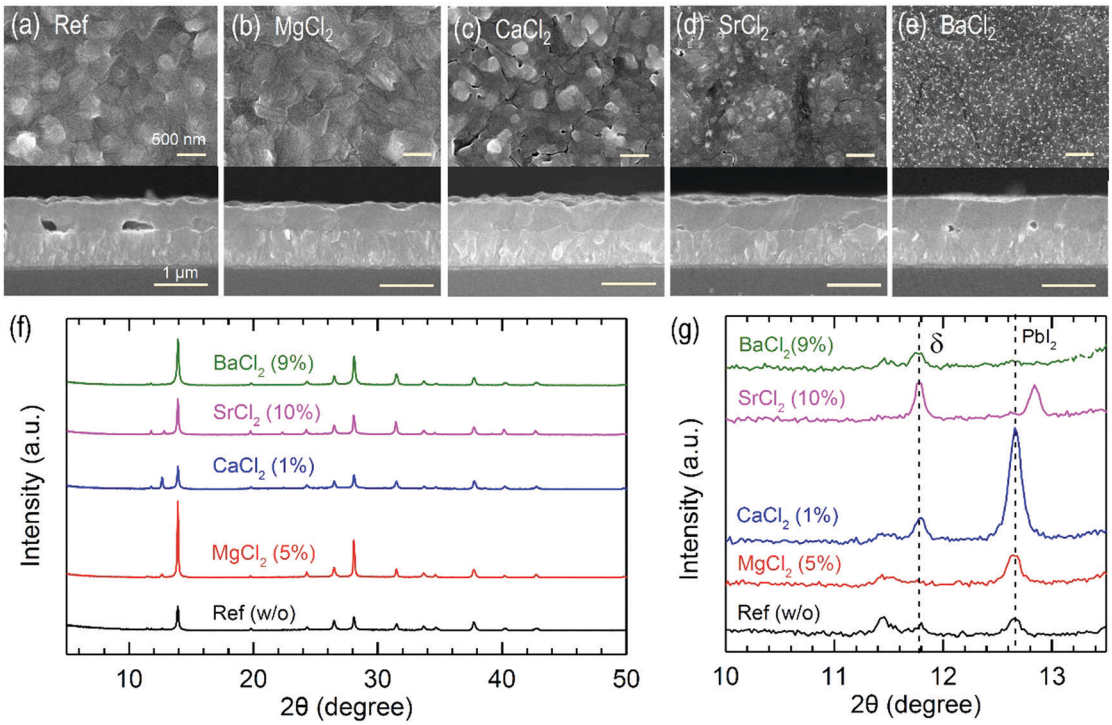

Fig. 3 (a–e) Top-view and cross-sectional scanning electron microscope (SEM) images and (f, g) X-ray diffraction patterns of $FAPbI_3$ films with and without (Ref) additives of $MgCl_2$, $CaCl_2$, $SrCl_2$ and $BaCl_2$.

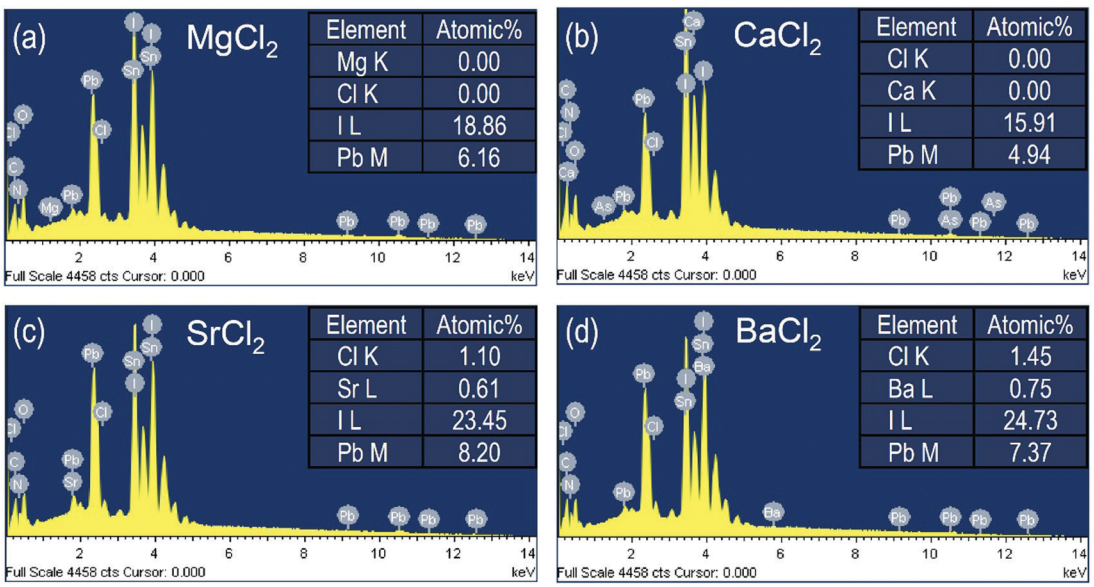

Fig. 4 Energy dispersive X-ray spectroscopy (EDS) of $FAPbI_3$ films with additive of (a) $MgCl_2$ (5%), (b) $CaCl_2$ (1%), (c) $SrCl_2$ (10%) and (d) $BaCl_2$ (9%).

(or Pb-deficient) phase is formed for $CaCl_2$ and $BaCl_2$ because of the ratio I/Pb = 3.22 ($CaCl_2$) and 3.35 ($BaCl_2$). Addition of $SrCl_2$ results in iodide-deficient (or Pb-rich) phase in the annealed perovskite film. Although excess PbI_2 or organic iodide was reported to passivate the perovskite grain boundary and thereby improve the photovoltaic performance,[32,33] the stoichiometry of the perovskite was also reported to play an important role in photovoltaic performance and stability because defects can be minimized by stoichiometric composition.[34] Thus, stoichiometric $FAPbI_3$ formed by $MgCl_2$ additive is in part responsible for the improved PCE. Since detection of $MgCl_2$ and $CaCl_2$ is unavailable by EDS, we further measure surface-sensitive X-ray photoelectron spectroscopy (XPS) to understand the chemical environment of $FAPbI_3$ films depending on additives.

Fig. 5(a–d) show Mg 1s, Ca 2p, Sr 3d and Ba 3d XPS spectra before and after addition of the additives. The film samples for

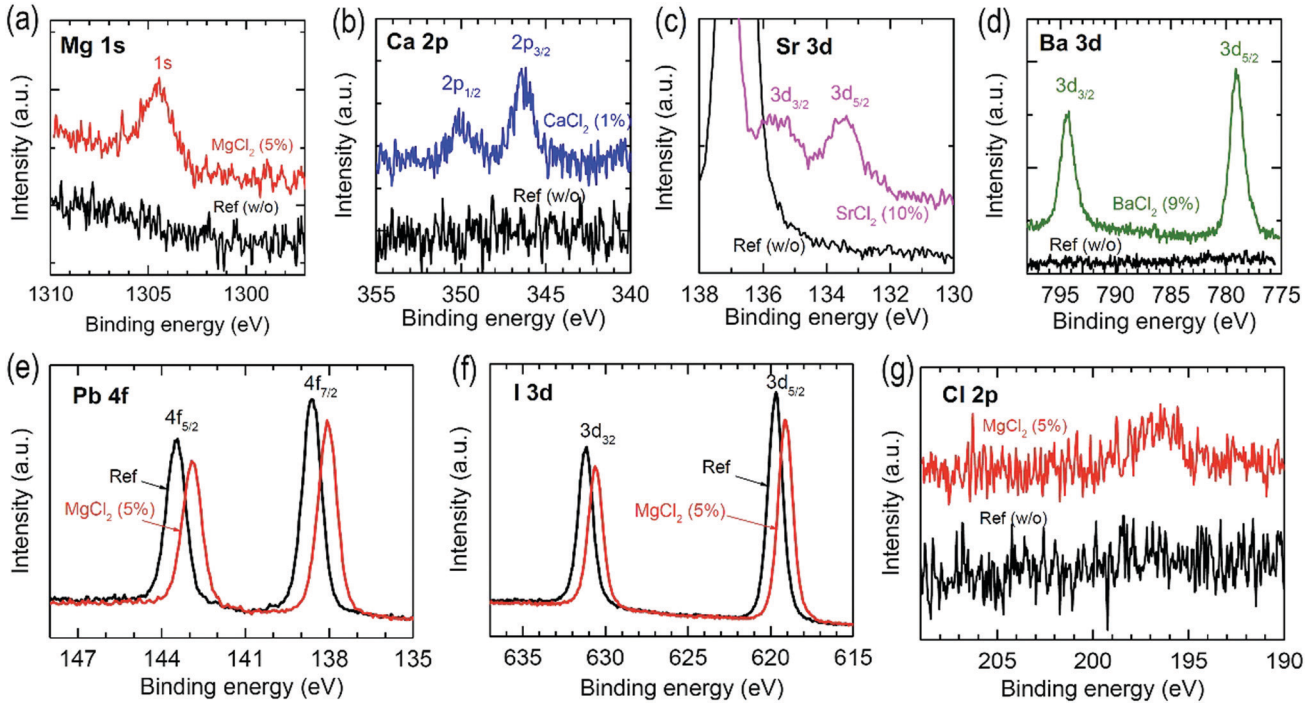

Fig. 5 Mg 1s, Ca 2p, Sr 3d and Ba 3d X-ray photoelectron spectroscopy (XPS) spectra of the annealed $FAPbI_3$ films with and without additives of (a) $MgCl_2$, (b) $CaCl_2$, (c) $SrCl_2$ and (d) $BaCl_2$. (e) Pb 4f, (f) I 3d and (g) Cl 2p XPS spectra of the $FAPbI_3$ films before and after adding the $MgCl_2$ additive.

XPS measurements were prepared on Si wafers. Mg, Ca, Sr and Ba elements are obviously detected. The detection of Cl from the $MgCl_2$-treated $FAPbI_3$ film confirms the existence of $MgCl_2$ in the film (see Fig. 5(g)). Thus, the additives still exist in the annealed perovskite films. Since addition of $MgCl_2$ significantly improved the photovoltaic performance among the studied BCl_2 additives, we further investigate Pb 4f and I 3d XPS for the $FAPbI_3$ films with and without $MgCl_2$. In Fig. 5(e), the pristine $FAPbI_3$ film shows two peaks at binding energies of 143.53 eV and 138.63 eV, which correspond to the Pb $4f_{5/2}$ and $4f_{7/2}$ core levels, respectively, originated from Pb^{2+} ions.[35,36] The addition of $MgCl_2$ in $FAPbI_3$ shifts the Pb 4f peaks to lower binding energies of 142.93 eV for $4f_{5/2}$ and 138.08 eV for $4f_{7/2}$. Shift to lower binding energy after adding $MgCl_2$ is also observed from I 3d XPS (Fig. 5(f)), where the $3d_{3/2}$ peak at 631.13 eV and the $3d_{5/2}$ peak at 619.68 eV shift to 630.63 eV and 619.13 eV. When considering no change in lattice constant by $MgCl_2$, Mg or Cl element might not be directly involved in lattice construction. Thus, the shift in binding energy is indicative of a change in chemical environment around Pb and I at the surface. The decrease in binding energy of Pb^{2+} and I^- is probably related to an increase in electron density around Pb^{2+} and I^-.[37–39] In the case that Mg^{2+} interacts with iodide at the surface, the (Pb–I) bond is more likely to be ionic due to an increased covalency of the adjacent (Mg–I) bond because of the smaller ionic radius of Mg^{2+} (72 pm) than Pb^{2+} (119 pm) according to Fajan's rule.[40] Thus, the electron density of iodide in the (Mg–I–Pb) interaction is relatively increased as compared to the (Pb–I–Pb) configuration. In addition, the more covalent character of (Mg–I) will donate electrons to Pb, which increases the electron density of Pb. Chloride in $MgCl_2$ can also affect the shift of the Pb 4f and the I 3d peaks by donating lone-pair elections to the perovskite surface. It was reported that post-treatment with $SrCl_2$ was found to shift the Pb 4f and the I 3d core levels to lower binding energy.[41]

Modification of the optical bandgap and band position is studied using UV-vis and ultraviolet photoelectron spectroscopy (UPS). Fig. 6(a) shows the UV-vis spectra of the annealed $FAPbI_3$ with and without additives. The absorbance is slightly enhanced by the additives, which is attributed to a slight increase in J_{sc}. Despite better absorbance observed from the $SrCl_2$ case, the lower J_{sc} than the reference device might be related to the presence of unconverted δ phase and/or poor SnO_2/perovskite interface in the aforementioned Fig. 3. The Tauc plot obtained from the UV-vis spectral data is shown in Fig. 6(b), where a linear fit in the 1.54–1.57 eV range of photon energy reveals that the optical bandgap (E_g) is determined to be 1.50 eV for $MgCl_2$ and $CaCl_2$ and 1.51 eV for $SrCl_2$ and $BaCl_2$, which are almost unchanged as compared to the pristine $FAPbI_3$ (E_g = 1.50 eV). Unaltered E_g is consistent with the invariable lattice constant as observed in XRD. Our result is different from the doping effect on E_g of $MAPbI_3$ or $CsPbI_3$, where E_g was influenced by doping due to the substitution effect.[42–45] Valence band (E_{VB}) and conduction band (E_{CB}) positions are determined from UPS using He I photon energy ($h\nu$ = 21.2 eV). In Fig. 6(c), UPS spectra are illustrated, showing the binding energy region of the cut-off energy (E_{cutoff}) and the valence band maximum (VBM). Work function (WF) is determined from WF = $h\nu - E_{cutoff}$ (see Fig. S3 (ESI†) for determining E_{cutoff}) and E_{VB} is determined using E_{VB} = WF + VBM (see Fig. S3 (ESI†) for determining VBM).[46] To determine

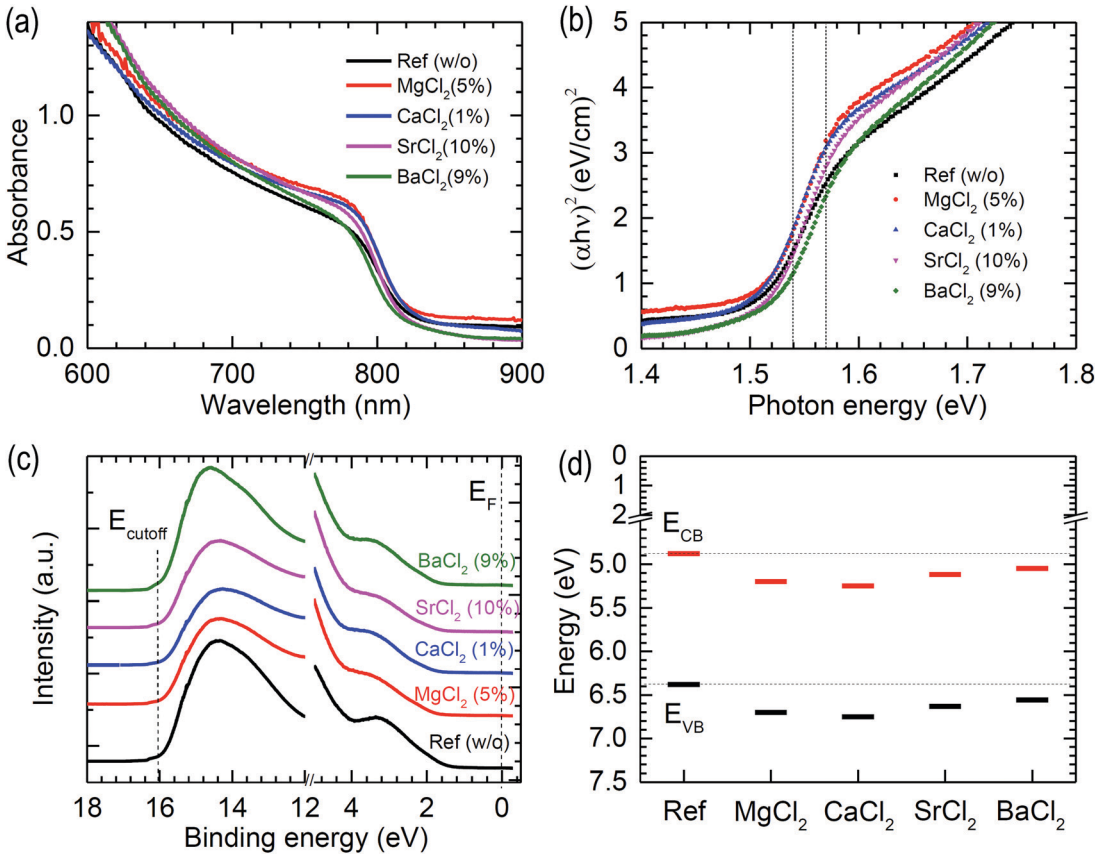

Fig. 6 (a) UV-vis spectra, (b) Tauc plot, (c) ultraviolet photoelectron spectroscopy (UPS) and (d) band (conduction band (CB) and valence band (VB)) positions for the $FAPbI_3$ films with and without additives. UPS spectra were measured with He I photon energy (21.2 eV).

Table 2 Work function (WF), valence band energy (E_{VB}) and conduction band energy (E_{CB}) estimated from the cut-off energy (E_{cutoff}), valence band maximum (VBM) and optical bandgap (E_g)

Sample	E_{cutoff} (eV)	WF (eV)	VBM (eV)	E_{VB} (eV)	E_g (eV)	E_{CB} (eV)
Ref (w/o)	16.05	5.15	1.23	6.38	1.50	4.88
$MgCl_2$ (5%)	16.05	5.15	1.55	6.70	1.50	5.20
$CaCl_2$ (1%)	16.00	5.20	1.55	6.75	1.50	5.25
$SrCl_2$ (10%)	16.02	5.18	1.45	6.63	1.51	5.12
$BaCl_2$ (9%)	16.11	5.09	1.47	6.56	1.51	5.05

VBM, we use a logarithmic scale method.[47] The estimated values are listed in Table 2 and plotted in Fig. 6(d). E_{VB} is determined to be 6.38 eV for the non-additive pristine $FAPbI_3$, which is consistent with the reported value obtained from the combined experimental and theoretical data.[48] Upon addition of additives, WF is almost unchanged, which indicates that the additive might not act as a dopant. Unlike the BI_2 additive in $MAPbI_3$ perovskite, resulting in up-shift of E_{VB} and E_{CB},[49] E_{VB} is down-shifted by the BCl_2 additives in $FAPbI_3$ perovskite films. The chloride seems to play a common effect on down-shifting E_{VB}. Since the antibonding-nature E_{VB} for the pristine $FAPbI_3$ is formed by overlapping the Pb 6s orbital with the I 5p from the viewpoint of molecular orbital theory, the chloride at the surface is likely to lower the E_{VB} because of overlap with a more electronegative Cl 3p orbital.[50] It was reported that a low concentration of Mg doping into $MAPbI_3$ led to down-shift of E_{VB} and more n-type property.[51] Thus, more n-type $FAPbI_3$ might be induced by addition of $MgCl_2$.

Effect of $MgCl_2$ additive on carrier mobility and trap density of $FAPbI_3$

The improved V_{oc} by $MgCl_2$ additive in spite of the unchanged E_g underlines that carrier lifetime, associated with trap density, is probably improved. To verify this hypothesis, we measure time-resolved photoluminescence (TRPL) along with steady-state PL. In Fig. 7(a), the PL intensity of the bulk perovskite film is increased by $MgCl_2$, which is indicative of reduction of non-radiative recombination. Upon contacting the perovskite film with SnO_2, the PL intensity is similarly decreased by 90.4% (pristine) and 89.5% ($MgCl_2$). Despite a similar degree of PL quenching, a lower J_{sc} for the pristine $FAPbI_3$ is due to the presence of pinholes at the SnO_2/perovskite interface (see Fig. 3). The TRPL spectrum in Fig. 7(b) is fit with the bi-exponential decay equation, $f(t) = A_1 \exp(-t/\tau_1) + A_2 \exp(-t/\tau_2)$, where τ_1 and τ_2 are time constants and A_1 and A_2 are amplitude.[33] Table 3 lists the fit results of pristine perovskite and perovskite film with $MgCl_2$ additive on the glass substrate. The addition of $MgCl_2$ increases τ_1 from 1.9 ns to 3.9 ns and τ_2 from 201.2 ns to 376.5 ns. In addition, the amplitude ratio (A_1/A_2) decreases significantly from 447.9 to 30.3 after addition of $MgCl_2$. This decrease in A_1/A_2 indicates that the contribution of the

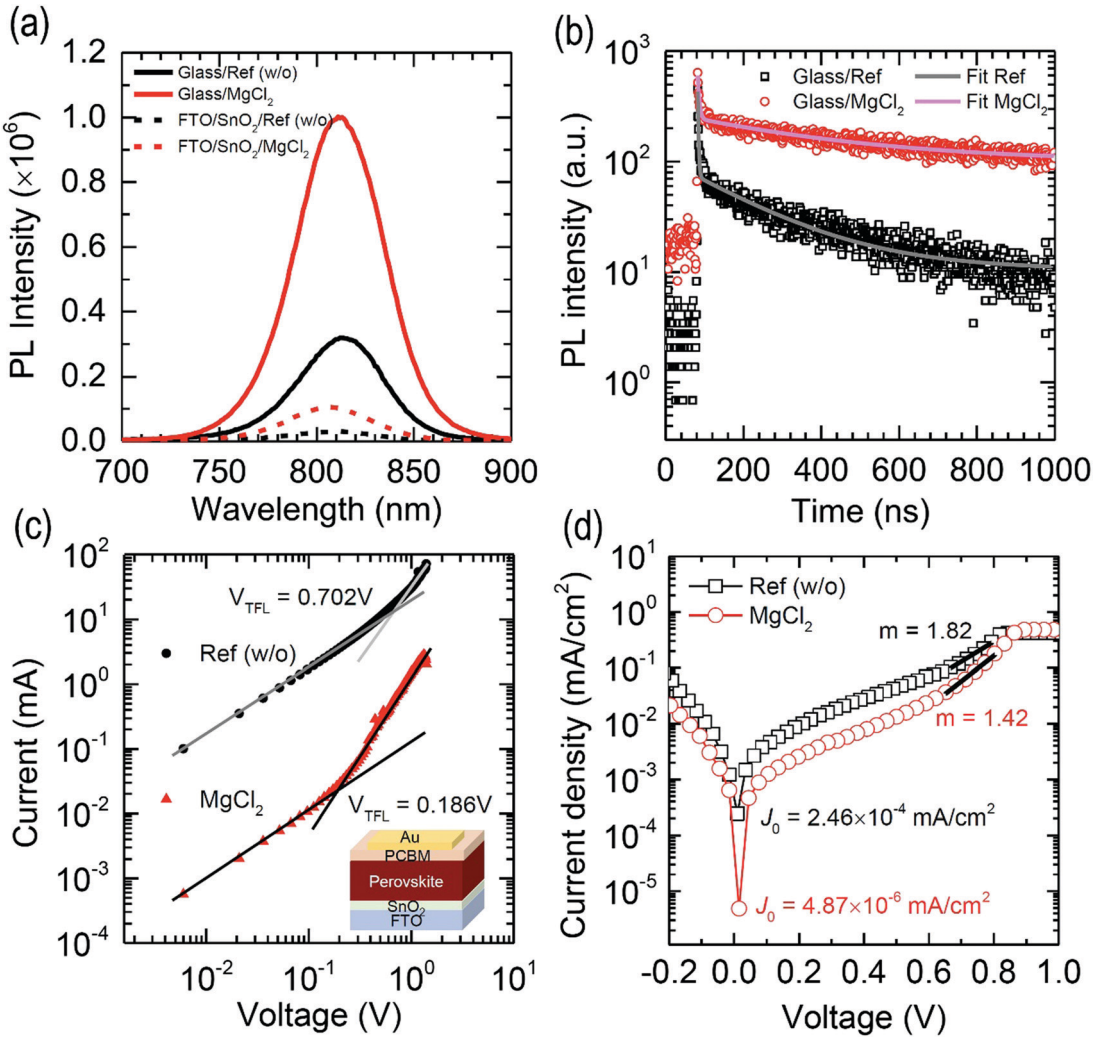

Fig. 7 (a) Steady-state photoluminescence (PL) of the $FAPbI_3$ film with and without $MgCl_2$ deposited on a glass substrate and SnO_2-coated FTO substrate. (b) Time-resolved PL (TRPL) for the $FAPbI_3$ film with and without $MgCl_2$ on a glass substrate. Dark current density (J)–voltage (V) curves for (c) the FTO/SnO_2/$FAPbI_3$ (with or without $MgCl_2$)/PCBM/Au electron-only device and (d) the full solar cell device.

Table 3 Parameters for fitting TRPL data with a bi-exponential decay equation of $f(t) = A_1\exp(-t/\tau_1) + A_2\exp(-t/\tau_2)$. Average lifetime ($\tau_{ave}$) was calculated by the weighted average of $(A_1\tau_1^2 + A_2\tau_2^2)/(A_1\tau_1 + A_2\tau_2)$

Samples	A_1	τ_1 (ns)	A_2	τ_2 (ns)	τ_{ave} (ns)
Glass/perovskite w/o $MgCl_2$	29111.5	1.9	65.0	201.2	40.1
Glass/perovskite w/$MgCl_2$	4545.8	3.9	150.2	376.5	287.6

recombination pathway associated with τ_1 decreases or in other words is mostly suppressed by the additive. Since τ_1 is the one related to the surface defects, whereas τ_2 is linked to bulk traps,[52] $MgCl_2$ appears to not only slow down the recombination process but suppress especially the presence of surface traps (*i.e.* the higher the number of surface traps, the larger the contribution (A_1)). As a result, average carrier lifetime (τ_{ave}) increases significantly from 40.1 ns to 287.6 ns after addition of $MgCl_2$. Trap density (n_t) is also evaluated from the space charge-limited current (SCLC) of a device with an electron-only configuration of FTO/SnO_2/perovskite/PCBM/Au[53] as shown in Fig. 7(c). n_t is calculated based on the trap-filled-limit voltage (V_{TFL}) obtained from dark J–V curves in Fig. 7(c).[15] V_{TFL} is estimated to be 0.702 V for the pristine $FAPbI_3$, which is significantly lowered to 0.186 V after the addition of $MgCl_2$. As a result, n_t decreases from 1.08×10^{16} cm^{-3}, which is consistent with the reported value,[54] to 3.19×10^{15} cm^{-3} after the addition of $MgCl_2$. The prolonged τ_{ave} is thus attributed to the decreased n_t. The reverse saturation current density (J_0) and the ideality factor (m) are also estimated from the full solar cell device structure in the dark. The dark J–V data shown in Fig. 7(d) result in $J_0 = 2.64 \times 10^{-4}$ mA cm^{-2} for the PSC employing the $FAPbI_3$ without additive, which is more than two orders of magnitude lowered after $MgCl_2$ ($J_0 = 4.87 \times 10^{-6}$ mA cm^{-2}). In addition, the addition of $MgCl_2$ lowers m from 1.82 to 1.42. The lower J_0 supports that the $MgCl_2$ additive in $FAPbI_3$ decreases shallow trap states. The reduced m is indicative of a suppression of the trap-assisted (mono molecular) recombination by the presence of $MgCl_2$ since the ideality factor correlates with the bimolecular band-to-band recombination (m = 1) and the Shockley–Read–Hall (SRH)

recombination (m = 2) in photoelectric devices.[55] The change in J_0 and m is also responsible for the improved V_{oc} and FF.[56,57]

Efficiency and stability of PSCs employing the $FAPbI_3$ film with $MgCl_2$ additive

Fig. 8(a) shows the J–V curves for the best performing PSCs employing the $FAPbI_3$ films with and without 5 mol% $MgCl_2$. The relevant photovoltaic parameters obtained from RS and FS are listed in Table 4. The PCE estimated from RS is enhanced from 17.27% to 21.11% after addition of 5 mol% $MgCl_2$ in the $FAPbI_3$ precursor solution due to the increment of V_{oc} from 1.06 V to 1.15 V, FF from 0.73 to 0.79 and J_{sc} from 22.39 mA cm^{-2} to 23.33 mA cm^{-2}. The integrated J_{sc}s from the EQE data in Fig. 8(b) show a slight deviation from the measured J_{sc} values but the same tendency (20.07 mA cm^{-2} without additive *vs.* 22.32 mA cm^{-2} with $MgCl_2$ additive). It is found from the steady-state J_{sc} and PCE measured at the maximum power point (MPP) that J_{sc} and PCE remain almost unchanged after 1500 s (Fig. 8(c)). This indicates that the $MgCl_2$ additive improves not only the efficiency but also the stability due to reduced bulk and surface defects simultaneously.

Table 4 Photovoltaic parameters of the best performing PSCs employing $FAPbI_3$ with and without 5 mol% $MgCl_2$ additive. FS and RS stand for forward scan and reverse scan, respectively

		J_{sc} (mA cm^{-2})	V_{oc} (V)	FF	PCE (%)
Ref (w/o)	FS	22.41	1.07	0.74	17.74
	RS	22.39	1.06	0.73	17.27
$MgCl_2$ (5%)	FS	23.33	1.13	0.78	20.58
	RS	23.33	1.15	0.79	21.11

Conclusions

We have demonstrated that the addition of $MgCl_2$ in the $FAPbI_3$ precursor solution substantially improved the photovoltaic performance without altering the bandgap and lattice constant. It was also found that the concentration of the additive played an important role in determining the photovoltaic

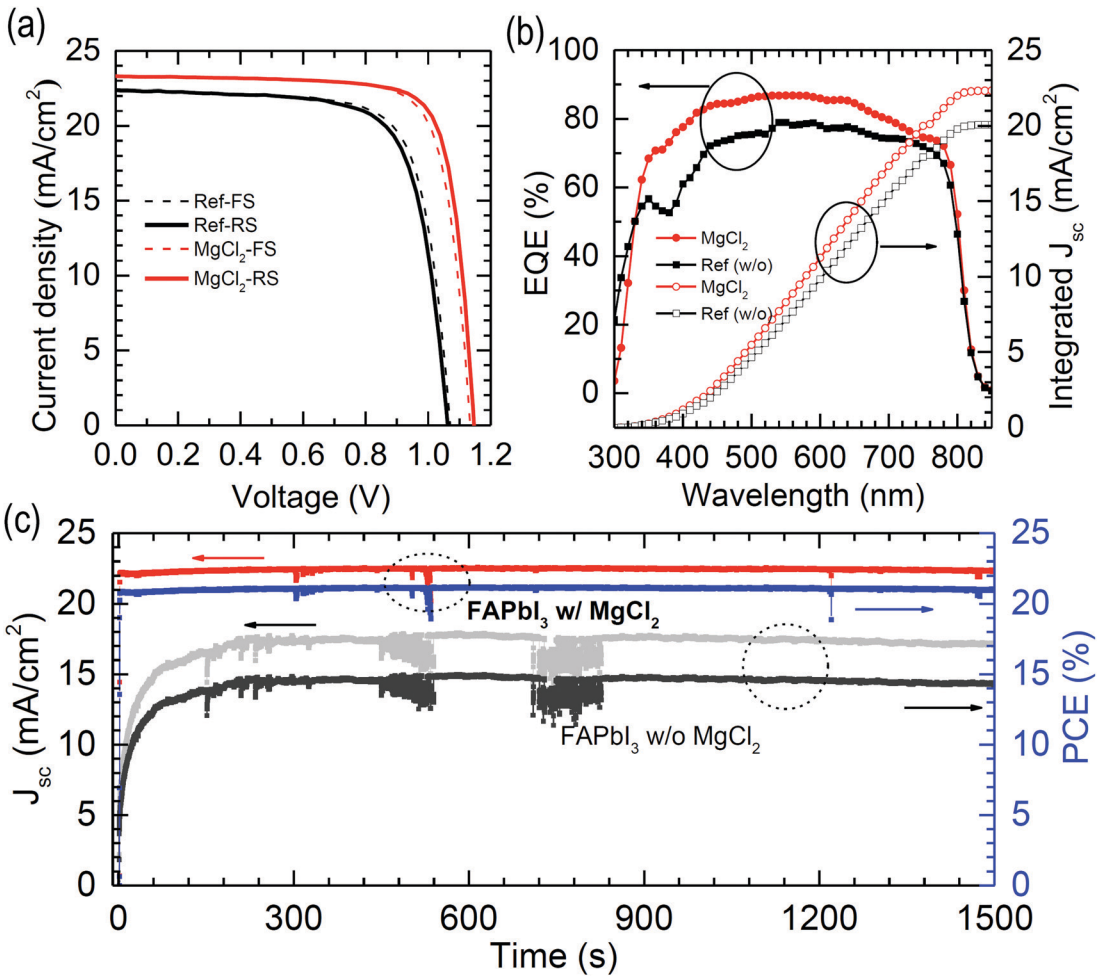

Fig. 8 (a) J–V curves and (b) external quantum efficiency (EQE) of PSCs employing $FAPbI_3$ with and without $MgCl_2$ additive. (c) Steady-state J_{sc} and PCE for the PSCs employing $FAPbI_3$ with and without the $MgCl_2$ additive, measured at the maximum power point (MPP) for 1500 s under continuous 1 sun illumination.

performance. $CaCl_2$ and $BaCl_2$ were found to increase the photovoltaic performance but the increment was marginal. For $SrCl_2$, the addition of $SrCl_2$ showed a negative effect due to poor morphology and incomplete $\delta \rightarrow \alpha$ phase transition. Using a nominal concentration of 5 mol% of $MgCl_2$, a photostable and 21.11% efficient PSC was achieved.

Experimental details

Materials

N,*N*-Dimethylformamide (DMF, 99.8%), dimethyl sulfoxide (DMSO, 99.9%), diethyl ether (99.7%), chlorobenzene (CB, 99.8%), formamidinium acetate (FAAc, 99%), lithium bis(trifluoromethanesulfonyl)imide (LiTFSI, 99.8%), 4-*tert*-butylpyridine (*t*BP, 98%), acetonitrile (ACN, 99.999%), hydroiodic acid (HI, 57 wt% in water), magnesium chloride ($MgCl_2$, 99.99%), calcium chloride ($CaCl_2$, 99.9%), strontium chloride ($SrCl_2$, 99.99%) and barium chloride ($BaCl_2$, 99.999%) were purchased from Sigma-Aldrich. Aqueous colloidal tin(IV) oxide solution (SnO_2, 15% in H_2O) was purchased from Alfa Aesar. 2,2′,7,7′-tetrakis(*N*,*N*′-di-*p*-methoxyphenylamine)-9,9′-spirobifluorene (spiro-MeOTAD) was purchased from Share-Chem. Lead(II) iodide (PbI_2, 95%) was purchased from Kanto Chemical Co., Inc. All the chemicals were used as-received without further purification. Fluorine doped tin oxide (FTO) glass (Pilkington, TEC-8, 8 Ω sq^{-1}) was used as a transparent electrode.

Synthesis of formamidinium iodide (FAI)

FAI was synthesized by reacting FAAc with HI. HI was slowly dropped into a round-bottom flask filled with FAAc, which was stirred for 2 h at 0 °C. The product was recovered by evaporating the solvent at 60 °C using a rotary evaporator, which was washed with diethyl ether and recrystallized from ethanol. Finally, the white precipitate was dried in a vacuum oven at 65 °C for 24 h and then stored in a glove box filled with argon prior to use.

Synthesis of $FAPbI_3$ powder

$FAPbI_3$ powder was synthesized by reacting FAI (2.236 g) with PbI_2 (4.61 g) (molar ratio FAI : PbI_2 = 1.3 : 1) in 60 ml ACN under stirring for 2 days at room temperature.[20] The product was dried in a vacuum oven for 2 days at room-temperature and then stored in a glove box filled with argon.

Device fabrication

FTO-coated glass was cleaned with solvents (water and ethanol), and was further treated with ultraviolet-ozone (UVO) for 40 min. A SnO_2 thin layer was prepared by spin-coating the diluted SnO_2 solution on the cleaned FTO substrate at 4000 rpm for 20 s and then annealed at 185 °C for 30 min. The SnO_2-coated FTO substrate was treated with UVO for 20 min prior to deposition of the perovskite precursor. The perovskite precursor solution was prepared by dissolving the pre-synthesized $FAPbI_3$ powder (concentration was 1.4 M) in a mixed solvent of DMF and DMSO (DMF : DMSO = 8 : 1 v/v). To study the effect of the additives, a certain amount of additive ($MgCl_2$ (5%): 0.0033 g, $CaCl_2$ (1%): 0.0008 g, $SrCl_2$ (10%): 0.0111 g, and $CaCl_2$ (9%): 0.0131 g) was mixed with 0.4431 g of $FAPbI_3$ powder in 0.5 ml of DMF/DMSO mixed solvent, which was stirred for over 12 h. It should be noted that $MgCl_2$ itself was dissolved well in the mixed DMF/DMSO solvent but a precipitate was partially formed when it was mixed with $FAPbI_3$. Thus filtration was required especially for the $MgCl_2$ case. For the perovskite deposition, the spin-coating condition was as follows. The precursor solution was filtered and 25 μl of precursor solution was spread on a SnO_2/FTO substrate, which was spun at 1000 rpm for 5 s and 5000 rpm for 20 s. Diethyl ether (1 ml) was dripped 20 s after spinning. The as-spun film was annealed at 150 °C for 30 min. A spiro-MeOTAD hole transporting layer was formed on the perovskite film by spin coating 20 μl of the spiro-MeOTAD solution (72.3 mg of spiro-MeOTAD, 28.8 μl of *t*BP, and 17.5 μl of LiTFSI solution (520 mg LiTSFI in 1 ml ACN in 1 mL of CB)) at 4000 rpm for 20 s. On top of the spiro-MeOTAD layer, a *ca.* 65 nm-thick Au electrode was formed by a thermal evaporation method at an evaporation rate of 0.3 Å s^{-1} under *ca.* 3.8×10^{-7} Torr.

Characterization

Current density–voltage (*J*–*V*) curves were obtained by a solar simulator with a 450 W xenon lamp (Newport 6279 NS) and a Keithley 2400 source meter. The AM 1.5G one sun (100 mW cm^{-2}) was adjusted by the NREL-calibrated silicon reference solar cell with a KG-5 filter. The external quantum efficiency (EQE) was measured using an EQE system equipped with a 75 W xenon lamp (USHIO) as a white light source, where the monochromatic beam was generated by chopping the white light. Scanning electron microscopy (SEM) images were observed with field-emission scanning electron microscopy (JSM7000F). UV-vis spectra were recorded using a UV-vis spectrophotometer (Lambda 45, PerkinElmer). Steady-state photoluminescence (PL) and time-resolved photoluminescence (TRPL) spectra were measured using a fluorescence spectrometer (QuantaurusTau C11367-12, Hamamatsu) with excitation of a 464 nm laser (PLP-10, Humamatsu) pulsed at a frequency of 10 MHz for steady-state PL and 200 kHz for TRPL. X-ray diffraction (XRD) patterns were obtained by the diffractometer (Rigaku Smart lab SE) with monochromatic Cu Kα radiation (λ = 1.54056 Å) at a scan rate of 4° min^{-1}. X-ray photoelectron spectroscopy (XPS) and ultraviolet photoelectron spectroscopy (UPS) measurements were carried out on an ESCALAB 250 XPS system (Thermo Fisher Scientific) with Al Kα X-ray radiation (1486.6 eV) for XPS and He I (21.2 eV) for UPS.

Conflicts of interest

The authors declare no conflict of interest.

Acknowledgements

This work was supported by the National Research Foundation of Korea (NRF) grants funded by the Ministry of Science and ICT (MSIT) of Korea under contracts NRF-2012M3A6A7054861

(Global Frontier R&D Program on Center for Multiscale Energy System), NRF-2016M3D1A1027663 and NRF-2016M3D1A1027664 (Future Materials Discovery Program) and NRF-2015M1A2A2-053004 (Climate Change Management Program).

Notes and references

1 H.-S. Kim, C.-R. Lee, J.-H. Im, K.-B. Lee, T. Moehl, A. Marchioro, S.-J. Moon, R. Humphry-Baker, J.-H. Yum, J. E. Moser, M. Grätzel and N.-G. Park, Lead Iodide Perovskite Sensitized All-Solid-State Submicron Thin Film Mesoscopic Solar Cell with Efficiency Exceeding 9%, *Sci. Rep.*, 2012, **2**, 591.

2 A. Kojima, K. Teshima, Y. Shirai and T. Miyasaka, Organometal Halide Perovskites as Visible-Light Sensitizers for Photovoltaic Cells, *J. Am. Chem. Soc.*, 2009, **131**, 6050–6051.

3 J.-H. Im, C.-R. Lee, J.-W. Lee, S.-W. Park and N.-G. Park, 6.5% efficient perovskite quantum-dot-sensitized solar cell, *Nanoscale*, 2011, **3**, 4088–4093.

4 https://www.nrel.gov/pv/cell-efficiency.html, accessed on April 29, 2020.

5 W. A. Laban and L. Etgar, Depleted hole conductor-free lead halide iodide heterojunction solar cells, *Energy Environ. Sci.*, 2013, **6**, 3249–3253.

6 G. C. Xing, N. Mathews, S. Y. Sun, S. S. Lim, Y. M. Lam, M. Grätzel, S. Mhaisalkar and T. C. Sum, Long-Range Balanced Electron- and Hole-Transport Lengths in Organic-Inorganic $CH_3NH_3PbI_3$, *Science*, 2013, **342**, 344–347.

7 M. A. Green, A. Ho-Baillie and H. J. Snaith, The emergence of perovskite solar cells, *Nat. Photonics*, 2014, **8**, 506–514.

8 J.-W. Lee, D.-J. Seol, A.-N. Cho and N.-G. Park, High-Efficiency Perovskite Solar Cells Based on the Black Polymorph of $HC(NH_2)_2PbI_3$, *Adv. Mater.*, 2014, **26**, 4991–4998.

9 X. J. Zheng, C. C. Wu, S. K. Jha, Z. Li, K. Zhu and S. Priya, Improved Phase Stability of Formamidinium Lead Triiodide Perovskite by Strain Relaxation, *ACS Energy Lett.*, 2016, **1**, 1014–1020.

10 J.-W. Lee, D.-H. Kim, H.-S. Kim, S.-W. Seo, S. M. Cho and N.-G. Park, Formamidinium and Cesium Hybridization for Photo- and Moisture-Stable Perovskite Solar Cell, *Adv. Energy Mater.*, 2015, **5**, 1501310.

11 W. S. Yang, J. H. Noh, N. J. Jeon, Y. C. Kim, S. Ryu, J. Seo and S. I. Seok, High-performance photovoltaic perovskite layers fabricated through intramolecular exchange, *Science*, 2015, **348**, 1234–1237.

12 C. Mu, J. L. Pan, S. Q. Feng, Q. Li and D. S. Xu, Quantitative Doping of Chlorine in Formamidinium Lead Trihalide ($FAPbI(3-x)Cl(x)$) for Planar Heterojunction Perovskite Solar Cells, *Adv. Energy Mater.*, 2017, **7**, 1601297.

13 J.-W. Lee and N.-G. Park, Chemical Approaches for Stabilizing Perovskite Solar Cells, *Adv. Energy Mater.*, 2020, **10**, 1903249.

14 N.-G. Park and K. Zhu, Scalable fabrication and coating methods for perovskite solar cells and solar modules, *Nat. Rev. Mater.*, 2020, **5**, 333–350.

15 S.-G. Kim, J. Chen, J.-Y. Seo, D.-H. Kang and N.-G. Park, Rear-Surface Passivation by Melaminium Iodide Additive for Stable and Hysteresis-less Perovskite Solar Cells, *ACS Appl. Mater. Interfaces*, 2018, **10**, 25372–25383.

16 M. Mateen, Z. Arain, Y. Yang, X. Liu, S. Ma, C. Liu, Y. Ding, X. Ding, M. Cai and S. Dai, MACl-Induced Intermediate Engineering for High-Performance Mixed-Cation Perovskite Solar Cells, *ACS Appl. Mater. Interfaces*, 2020, **12**, 10535–10543.

17 M. Kim, G.-H. Kim, T. K. Lee, I. W. Choi, H. W. Choi, Y. Jo, Y. J. Yoon, J. W. Kim, J. Lee, D. Huh, H. Lee, S. K. Kwak, J. Y. Kim and D. S. Kim, Methylammonium Chloride Induces Intermediate Phase Stabilization for Efficient Perovskite Solar Cells, *Joule*, 2019, **3**, 2179–2192.

18 G. Yang, H. Zhang, G. Li and G. Fang, Stabilizer-assisted growth of formamdinium-based perovskites for highly efficient and stable planar solar cells with over 22% efficiency, *Nano Energy*, 2019, **63**, 103835.

19 B. Lee, T. Hwang, S. Lee, B. Shin and B. Park, Microstructural Evolution of Hybrid Perovskites Promoted by Chlorine and its Impact on the Performance of Solar Cell, *Sci. Rep.*, 2019, **9**, 4803.

20 Y. Zhang, S. Seo, S. Y. Lim, Y. Kim, S.-G. Kim, D.-K. Lee, S.-H. Lee, H. Shin, H. Cheong and N.-G. Park, Achieving Reproducible and High-Efficiency (>21%) Perovskite Solar Cells with a Presynthesized $FAPbI_3$ Powder, *ACS Energy Lett.*, 2020, **5**, 360–366.

21 G. S. Shin, S.-G. Kim, Y. Zhang and N.-G. Park, A Correlation between Iodoplumbate and Photovoltaic Performance of Perovskite Solar Cells Observed by Precursor Solution Aging, *Small Methods*, 2020, **4**, 1900398.

22 Y. Deng, C. H. V. Brackle, X. Dai, J. Zhao, B. Chen and J. Huang, Tailoring solvent coordination for high-speed, room-temperature blading of perovskite photovoltaic films, *Sci. Adv.*, 2019, **5**, eaax7537.

23 N. Ahn, D.-Y. Son, I.-H. Jang, S. M. Kang, M. Choi and N.-G. Park, Highly Reproducible Perovskite Solar Cells with Average Efficiency of 18.3% and Best Efficiency of 19.7% Fabricated via Lewis Base Adduct of Lead(II) Iodide, *J. Am. Chem. Soc.*, 2015, **137**, 8696–8699.

24 S.-H. Chan, M.-C. Wu, K.-M. Lee, W.-C. Chen, T.-H. Lina and W.-F. Su, Enhancing perovskite solar cell performance and stability by doping barium in methylammonium lead halide, *J. Mater. Chem. A*, 2017, **5**, 18044–18052.

25 M.-C. Wu, T.-H. Lin, S.-H. Chan, Y.-H. Liao and Y.-H. Chang, Enhanced Photovoltaic Performance of Perovskite Solar Cells by Tuning Alkaline Earth Metal-Doped Perovskite-Structured Absorber and Metal-Doped TiO_2 Hole Blocking Layer, *ACS Appl. Energy Mater.*, 2018, **1**, 4849–4859.

26 H. Zhang, H. Wang, S. T. Williams, D. Xiong, W. Zhang, C.-C. Chueh, W. Chen and A. K.-Y. Jen, $SrCl_2$ Derived Perovskite Facilitating a High Efficiency of 16% in Hole-Conductor-Free Fully Printable Mesoscopic Perovskite Solar Cells, *Adv. Mater.*, 2017, **29**, 1606608.

27 C. F. J. Lau, M. Zhang, X. Deng, J. Zheng, J. Bing, Q. Ma, J. Kim, L. Hu, M. A. Green, S. Huang and A. Ho-Baillie, Strontium-Doped Low-Temperature-Processed $CsPbI_2Br$ Perovskite Solar Cells, *ACS Energy Lett.*, 2017, **2**, 2319–2325.

28 F. Yang, M. A. Kamarudin, G. Kapil, D. Hirotani, P. Zhang, C. H. Ng, T. Ma and S. Hayase, Magnesium-Doped $MAPbI_3$

Perovskite Layers for Enhanced Photovoltaic Performance in Humid Air Atmosphere, *ACS Appl. Mater. Interfaces*, 2018, **10**, 24543–24548.

29 R. Chen, D. Hou, C. Lu, J. Zhang, P. Liu, H. Tian, Z. Zeng, Q. Xiong, Z. Hu, Y. Zhu and L. Han, Zinc ion as Effective Film Morphology Controller in Perovskite Solar Cells, *Sustainable Energy Fuels*, 2018, **2**, 1093–1100.

30 N. Guijarro, M. S. Prévot, X. Yu, X. A. Jeanbourquin, P. Bornoz, W. Bourée, M. Johnson, F. L. Formal and K. Sivula, A Bottom-Up Approach toward All-Solution-Processed High-Efficiency Cu(In,Ga)S_2 Photocathodes for Solar Water Splitting, *Adv. Energy Mater.*, 2016, **6**, 1501949.

31 G. S. Shin, Y. Zhang and N.-G. Park, Stability of Precursor Solution for Perovskite Solar Cell: Mixture (FAI + PbI_2) versus Synthetic $FAPbI_3$ Crystal, *ACS Appl. Mater. Interfaces*, 2020, **12**, 15167–15174.

32 H. Zhou, Q. Chen, G. Li, S. Luo, T.-B. Song, H.-S. Duan, Z. Hong, J. You, Y. Liu and Y. Yang, Interface engineering of highly efficient perovskite solar cells, *Science*, 2014, **345**, 542–546.

33 D.-Y. Son, J.-W. Lee, Y. J. Choi, I.-H. Jang, S. Lee, P. J. Yoo, H. Shin, N. Ahn, M. Choi, D. Kim and N.-G. Park, Self-formed grain boundary healing layer for highly efficient $CH_3NH_3PbI_3$ perovskite solar cells, *Nat. Energy*, 2016, **1**, 1–8.

34 L. K. Ono, S. (Frank) Liu and Y. Qi, Reducing Detrimental Defects for High-Performance Metal Halide Perovskite Solar Cells, *Angew. Chem. Int. Ed.*, 2020, **59**, 6676–6698.

35 J. Chen, J.-Y. Seo and N.-G. Park, Simultaneous Improvement of Photovoltaic Performance and Stability by In Situ Formation of 2D Perovskite at $(FAPbI_3)_{0.88}(CsPbBr_3)_{0.12}$/CuSCN Interface, *Adv. Energy Mater.*, 2018, **8**, 1702714.

36 M. Kot, M. Vorokhta, Z. Wang, H. J. Snaith, D. Schmeißer and J. I. Fleg, Thermal stability of $CH_3NH_3PbI_xCl_{3-x}$ versus $[HC(NH_2)_2]_{0.83}Cs_{0.17}PbI_{2.7}Br_{0.3}$ perovskite films by X-ray photoelectron spectroscopy, *Appl. Surf. Sci.*, 2020, **513**, 145596.

37 J. Chen, S.-G. Kim, X. Ren, H. S. Jung and N.-G. Park, Effect of bidentate and tridentate additives on the photovoltaic performance and stability of perovskite solar cells, *J. Mater. Chem. A*, 2019, **7**, 4977–4987.

38 H.-L. Hsu, H.-T. Hsiao, T.-Y. Juang, B.-H. Jiang, S.-C. Chen, R.-J. Jeng and C.-P. Chen, Perovskite Solar Cells: Carbon Nanodot Additives Realize High-Performance Air-Stable p–i–n Perovskite Solar Cells Providing Efficiencies of up to 20.2%, *Adv. Energy Mater.*, 2018, **8**, 1802323.

39 J. Li, T. Jiu, S. Chen, L. Liu, Q. Yao, F. Bi, C. Zhao, Z. Wang, M. Zhao and G. Zhang, Graphdiyne as a Host Active Material for Perovskite Solar Cell Application, *Nano Lett.*, 2018, **18**, 6941–6947.

40 K. Fajans, Struktur und Deformation der Elektronenhüllen in ihrer Bedeutung für die chemischen und optischen Eigenschaften anorganischer Verbindungen, *Naturwissenschaften*, 1923, **11**, 165–172.

41 S. Wang, H. Cao, X. Liu, Y. Liu, T. Tao, J. Sun and M. Zhang, Strontium Chloride Passivated Perovskite Thin Films for Efficient Solar Cells with Power Conversion Efficiency over 21% and Superior Stability, *ACS Appl. Mater. Interfaces*, 2020, **12**, 3661–3669.

42 M. Pazoki, T. J. Jacobsson, A. Hagfeldt, G. Boschloo and T. Edvinsson, Effect of metal cation replacement on the electronic structure of metalorganic halide perovskites: Replacement of lead with alkaline-earth metals, *Phys. Rev. B*, 2016, **93**, 144105.

43 J. Navas, A. Sánchez-Coronilla, J. J. Gallardo, N. C. Hernández, J. C. Piñero, R. Alcántara, C. Fernández-Lorenzo, D. M. D. l. Santos, T. Aguilar and J. Martín-Calleja, New insights into organic–inorganic hybrid perovskite $CH_3NH_3PbI_3$ nanoparticles. An experimental and theoretical study of doping in Pb^{2+} sites with Sn^{2+}, Sr^{2+}, Cd^{2+} and Ca^{2+}, *Nanoscale*, 2015, **7**, 6216–6229.

44 T. J. Jacobsson, M. Pazoki, A. Hagfeldt and T. Edvinsson, Goldschmidt's Rules and Strontium Replacement in Lead Halogen Perovskite Solar Cells: Theory and Preliminary Experiments on $CH_3NH_3SrI_3$, *J. Phys. Chem. C*, 2015, **119**, 25673–25683.

45 C. F. J. Lau, X. Deng, J. Zheng, J. Kim, Z. Zhang, M. Zhang, J. Bing, B. Wilkinson, L. Hu, R. Patterson, S. Huanga and A. Ho-Baillie, Enhanced performance via partial lead replacement with calcium for a $CsPbI_3$ perovskite solar cell exceeding 13% power conversion efficiency, *J. Mater. Chem. A*, 2018, **6**, 5580–5586.

46 B. Philippe, T. J. Jacobsson, J.-P. Correa-Baena, N. K. Jena, A. Banerjee, S. Chakraborty, U. B. Cappel, R. Ahuja, A. Hagfeldt, M. Odelius and H. Rensmo, Valence Level Character in a Mixed Perovskite Material and Determination of the Valence Band Maximum from Photoelectron Spectroscopy: Variation with Photon Energy, *J. Phys. Chem. C*, 2017, **121**, 26655–26666.

47 J. Endres, D. A. Egger, M. Kulbak, R. A. Kerner, L. Zhao, S. H. Silver, G. Hodes, B. P. Rand, D. Cahen, L. Kronik and A. Kahn, Valence and Conduction Band Densities of States of Metal Halide Perovskites: A Combined Experimental-Theoretical Study, *J. Phys. Chem. Lett.*, 2016, **7**, 2722–2729.

48 S. Tao, I. Schmidt, G. Brocks, J. Jiang, I. Tranca, K. Meerholz and S. Olthof, Absolute energy level positions in tinand lead-based halide perovskites, *Nat. Commun.*, 2019, **10**, 1–10.

49 C. Lu, J. Zhang, D. Hou, X. Gan, H. Sun, Z. Zeng, R. Chen, H. Tian, Q. Xiong, Y. Zhang, Y. Li and Y. Zhu, Calcium doped $MAPbI_3$ with better energy state alignment in perovskite solar cells, *Appl. Phys. Lett.*, 2018, **112**, 193901.

50 W.-J. Yin, H. Chen, T. Shi, S.-H. Wei and Y. Yan, Origin of High Electronic Quality in Structurally Disordered $CH_3NH_3PbI_3$ and the Passivation Effect of Cl and O at Grain Boundaries, *Adv. Electron. Mater.*, 2015, **1**, 1500044.

51 N. Phung, R. Félix, D. Meggiolaro, A. Al-Ashouri, G. S. E. Silva, C. Hartmann, J. Hidalgo, H. Köbler, E. Mosconi, B. Lai, R. Gunder, M. Li, K.-L. Wang, Z.-K. Wang, K. Nie, E. Handick, R. G. Wilks, J. A. Marquez, B. Rech, T. Unold, J.-P. Correa-Baena, S. Albrecht, F. D. Angelis, M. Bär and A. Abate, The Doping Mechanism of Halide Perovskite Unveiled by Alkaline Earth Metals, *J. Am. Chem. Soc.*, 2020, **142**, 2364–2374.

52 Y. Zhang, S.-G. Kim, D. Lee, H. Shin and N.-G. Park, Bifacial stamping for high efficiency perovskite solar cells, *Energy Environ. Sci.*, 2019, **12**, 308–321.

53 D. Yang, X. Zhou, R. Yang, Z. Yang, W. Yu, X. Wang, C. Li, S. (Frank) Liu and R. P. H. Chang, Surface optimization to

eliminate hysteresis for record efficiency planar perovskite solar cells, *Energy Environ. Sci.*, 2016, **9**, 3071–3078.

54 D.-Y. Son, S.-G. Kim, J.-Y. Seo, S.-H. Lee, H. Shin, D. Lee and N.-G. Park, Universal approach toward hysteresis-free perovskite solar cell via defect engineering, *J. Am. Chem. Soc.*, 2018, **140**, 1358–1364.

55 T. He, S. Li, Y. Jiang, C. Qin, M. Cui, L. Qiao, H. Xu, J. Yang, R. Long, H. Wang and M. Yuan, Reduced-dimensional perovskite photovoltaics with homogeneous energy landscape, *Nat. Commun.*, 2020, **11**, 1672.

56 W. Tress, Perovskite Solar Cells on the Way to Their Radiative Efficiency Limit-Insights Into a Success Story of High Open-Circuit Voltage and Low Recombination, *Adv. Energy Mater.*, 2017, **7**, 1602358.

57 N.-G. Park and H. Segawa, Research Direction toward Theoretical Efficiency in Perovskite Solar Cells, *ACS Photonics*, 2018, **5**, 2970–2977.